Progress In Electromagnetics Research B, Vol. 12, 105–138, 2009

ELECTROMAGNETIC TRANSMISSION THROUGH FRACTAL APERTURES IN INFINITE CONDUCTING SCREEN

B. Ghosh, S. N. Sinha, and M. V. Kartikeyan

Department of Electronics and Computer Engineering
Indian Institute of Technology
Roorkee-247667, India

Abstract—Fractals contain an infinite number of scaled copies of a starting geometry. Due to this fundamental property, they offer multiband characteristics and can be used for miniaturization of antenna structures. In this paper, electromagnetic transmission through fractal shaped apertures in an infinite conducting screen has been investigated for a number of fractal geometries like Sierpinski gasket, Sierpinski carpet, Koch curve, Hilbert Curve and Minkowski fractal. Equivalence principle and image theory are applied to obtain an operator equation in terms of equivalent surface magnetic current over the aperture surface. The operator equation is then solved using method of moments (MoM) with the aperture surface modeled using triangular patches. Numerical results are presented in terms of transmission coefficient and transmission cross-section for both parallel and perpendicular polarizations of incident plane wave which show the existence of multiple transmission bands.

1. INTRODUCTION

The problem of electromagnetic coupling between two regions via apertures in conducting screens has been the subject of interest to researchers for many years due to their applications in frequency selective surfaces (FSS), antenna arrays, and electromagnetic interference and compatibility. The electromagnetic field coupling through small apertures and arrays of apertures in conducting screens illuminated by a plane wave has been analyzed in [1–3]. The transmission characteristics of multiple apertures of rectangular and

Corresponding author: B. Ghosh (basugdec@iitr.ernet.in).

circular shape in a thick conducting screen have been analyzed in [4, 5] using the Fourier transform and mode matching methods. A thin conducting screen perforated with multiple apertures has a band pass characteristics when illuminated by a plane wave of varying frequency. This makes it a useful candidate in the design of microwave filters, FSS, electromagnetic band gap (EBG) materials, bandpass radoms, artificial dielectric and antenna reflectors or ground planes [6].

Over last few years, fractal geometries have been widely used in the design of antennas and frequency selective surfaces (FSS). A comprehensive review of the applications of fractals in electromagnetics can be found in [7]. Due to their self similar properties, the fractal based frequency selective surfaces offer multiple bands. Also, due to their space filling properties, they can be used to miniaturize the dimensions of the unit cell. A dual-band fractal FSS based on Sierpinski gasket was reported in [8]. Various frequency selective surfaces based on self-similar prefractals for multiband and dual-polarized applications can be found in [9]. A high impedance metamaterial surface based on Hilbert curve has been shown to have a reflection coefficient $\Gamma \simeq +1$, when illuminated by a plane wave [10].

Photonic band gap structures are capable of reflecting the electromagnetic waves at a selected frequency and are conveniently constructed by using a periodic arrangement of dielectric materials. The dimension of the photonic band gap structures has to be few times the wavelength of the point of total reflection which makes it very large for larger wavelength applications, especially in microwave frequency regime. Frequency selective surfaces are also capable of totally reflecting the incident electromagnetic wave. However, the frequency of total reflection is determined by the lateral dimension of unit cell and hence, it requires a larger surface area. On the other hand, it was shown in [11, 12] that the planar metallic fractal can reflect electromagnetic wave at a wavelength much larger than the dimension of sample size. The fractal pattern shows a quasi log periodic behavior for lower order iterations of fractal geometry, and the response becomes log periodic for large number of iterations. It was pointed out in [13] that the increase in number of iterations downshifts the passbands, as well as, the stop bands. A fractal slit based on the same fractal geometry was analyzed in [14], where, it was pointed out that the fractal slit supports the subwavelength transmission of electromagnetic waves.

In this paper, we numerically investigate the problem of electromagnetic transmission through fractal apertures in a thin infinite conducting screen illuminated by a plane wave. The basic technique used in the analysis is based upon the '*generalized network*

formulation for aperture problems' using method of moments [15]. First, the equivalence principle is applied to divide the problem into two equivalent problems — one for each region. The boundary conditions are invoked on the aperture surface to obtain the operator equation in terms of equivalent surface magnetic current density. The integral equation is then solved using the method of moments with RWG functions [16]. Near-field and far-field behavior of fractal apertures are characterized in terms of transmission coefficient and transmission cross-section, respectively.

2. FORMULATION OF THE PROBLEM

The general problem of electromagnetic transmission through multiple arbitrarily-shaped apertures in an infinite conducting screen is shown in Fig. 1. The apertures are assumed to be in $z = 0$ plane. An arbitrarily polarized plane wave is incident on the aperture from $z < 0$ region making an angle θ_i with z-axis. The medium for region 'a' ($z < 0$) is characterized by (μ_a, ε_a) and region 'b' ($z > 0$) by (μ_b, ε_b). Equivalence principle is applied to separate the original problem into two equivalent problems. As shown in Fig. 2, the apertures $A_1, A_2, \ldots, A_N$ are closed by perfect electric conductors (PEC) and equivalent surface magnetic currents $+\overline{M}$ and $-\overline{M}$ are placed over the aperture regions on opposite sides to ensure the continuity of tangential component of electric field. The surface magnetic current is defined as $\overline{M} = \hat{n} \times \overline{E}$ where $\hat{n}$ is the unit outward normal and $\overline{E}$ is the

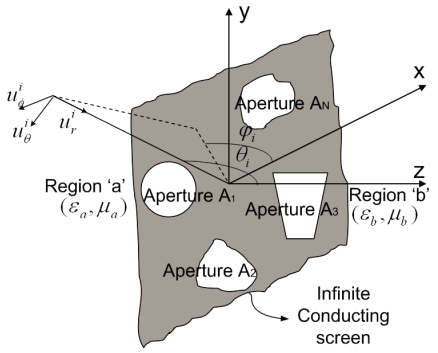

Figure 1. General problem geometry of multiple arbitrarily shaped apertures in an infinite conducting screen.

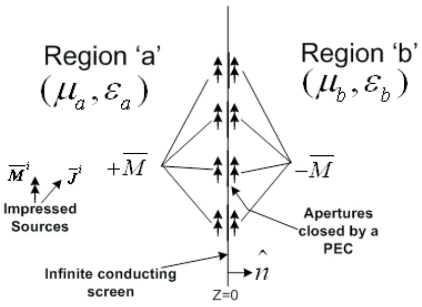

Figure 2. Equivalent problem after the application of equivalence principle.

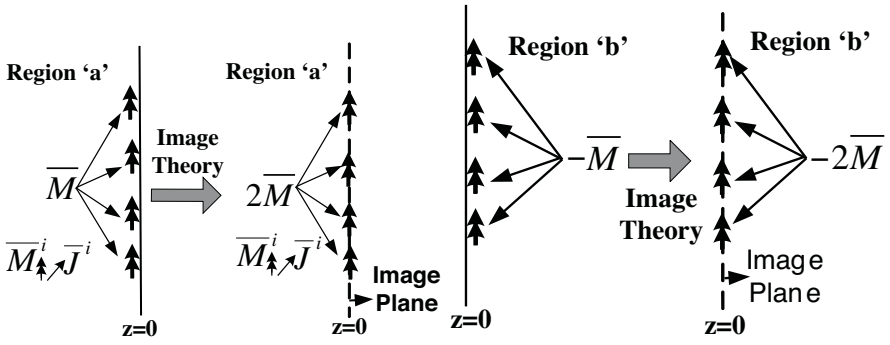

(a) Region $z < 0$ (b) Region $z > 0$

Figure 3. Equivalent problem after the application of image theory.

electric field on the apertures of original problem. Now, image theory is applied to further simplify the equivalent problems for the two regions, as shown in Fig. 3. The general formulation of the problem is the same as that described in [17], except for the calculation of singular integrals. Expanding $\overline{M}$ as $\overline{M} = \sum_{n=1}^{N} V_n \overline{M}_n$, and applying the method of moments, the problem can be expressed in terms of the following matrix equation:

$$[Y]\overrightarrow{V} = \overrightarrow{I}^{i} \tag{1}$$

where

$$[Y] = 4\left[\left\langle -\overline{W}_m, \overline{H}_t^{fs}\left(\overline{M}_n\right)\right\rangle\right]_{N\times N} \tag{2}$$

$$\overrightarrow{I}^{i} = 2\left[\left\langle \overline{W}_m, \overline{H}_t^{io}\right\rangle\right]_{N\times 1} \tag{3}$$

and

$$V = [V_n]_{N\times 1} \tag{4}$$

Here, $\overline{W}_m$ and $\overline{M}_n$ are the mth and nth weighting and basis functions, respectively, $\overline{H}_t^{fs}(\overline{M}_n)$ is the tangential component of magnetic field on the apertures due to an equivalent surface magnetic current $\overline{M}_n$ radiating in free space, and $\overline{H}_t^{io}$ is the tangential component of magnetic field over the apertures due to an incident plane wave. Using Galerkin's method, i.e., $\overline{W}_m = \overline{M}_m$, the admittance

matrix can be expressed as

$$Y_{mn} = 4\left\langle -\overline{M}_m, \overline{H}_t^{fs}\left(\overline{M}_n\right)\right\rangle \tag{5}$$

Following the procedure described in [17], an element of admittance matrix can be expressed in terms of RWG function over the nth source triangle with observation point at the centroid of mth triangle as

$$Y_{mn} = \frac{j\omega\varepsilon l_m l_n}{4\pi}\left\{\begin{array}{l} \overline{\rho}_m^{c+}(\overline{r})\cdot\frac{1}{A_n^+}\iint_{T_n^+}\overline{\rho}_n^+(\overline{r}\,')\,G(\overline{r}_m^{c+}|\overline{r}\,')\,ds' \\ +\overline{\rho}_m^{c+}(\overline{r})\cdot\frac{1}{A_n^-}\iint_{T_n^-}\overline{\rho}_n^-(\overline{r}\,')\,G(\overline{r}_m^{c+}|\overline{r}\,')\,ds' \\ +\overline{\rho}_m^{c-}(\overline{r})\cdot\frac{1}{A_n^+}\iint_{T_n^+}\overline{\rho}_n^+(\overline{r}\,')\,G(\overline{r}_m^{c-}|\overline{r}\,')\,ds' \\ +\overline{\rho}_m^{c-}(\overline{r})\cdot\frac{1}{A_n^-}\iint_{T_n^-}\overline{\rho}_n^-(\overline{r}\,')\,G(\overline{r}_m^{c-}|\overline{r}\,')\,ds' \end{array}\right\}$$
$$+\frac{l_m l_n}{\pi j\omega\mu}\left\{\begin{array}{l} \frac{1}{A_n^+}\iint_{T_n^+}G(\overline{r}_m^{c+}|\overline{r}\,')\,ds' - \frac{1}{A_n^-}\iint_{T_n^-}G(\overline{r}_m^{c+}|\overline{r}\,')\,ds' \\ -\frac{1}{A_n^+}\iint_{T_n^+}G(\overline{r}_m^{c-}|\overline{r}\,')\,ds' + \frac{1}{A_n^-}\iint_{T_n^-}G(\overline{r}_m^{c-}|\overline{r}\,')\,ds' \end{array}\right\} \tag{6}$$

where l_m and l_n are the lengths of the mth and nth edges shared by triangle pairs $T_m^{\pm}$ and $T_n^{\pm}$, respectively and $G(\overline{r}|\overline{r}\,')$ is the free space Green's function which is given by $G(\overline{r}|\overline{r}\,') = \frac{\exp(-jk|r-r'|)}{|r-r'|}$.

Equation (6) involves integrals of the following form

$$\overline{F}_{pq}^{j} = \iint_{T_q}\overline{\rho}_j\left(\overline{r}\,'\right)G\left(\overline{r}_p|\overline{r}\,'\right)ds' \qquad \begin{array}{r} p,q = 1,2,3,\ldots,P \\ j = 1,2,3 \end{array} \tag{7}$$

and

$$\varphi_{pq} = \iint_{T_q} G\left(\overline{r}_p|\overline{r}\,'\right)ds'; \qquad p,q = 1,2,3,\ldots,P \tag{8}$$

where P is the total number of triangles. Integrals in (7) and (8) are singular when the source and observation triangles coincide i.e., $p = q$ and hence, require some special numerical considerations for their evaluation. A number of research works have been reported based on singularity subtraction approach [13–16]. However, as has been pointed out in [22], a singularity cancellation method is not only more accurate but also has the advantage that the integrals can be evaluated using purely numerical quadrature schemes. Therefore, the singularity cancellation method proposed in [22] has been used in this paper. Once the integrals are calculated and stored, the complete

admittance matrix can be expressed in the following form

$$Y_{mn} = \frac{j\omega\varepsilon l_m l_n}{4\pi}\left\{\begin{array}{c} \frac{1}{A_n^+}\overline{\rho}_m^{c+}\cdot\overline{F}_{p(m^+)q(n^+)}^{j(n^+)} - \frac{1}{A_n^-}\overline{\rho}_m^{c+}\cdot\overline{F}_{p(m^+)q(n^-)}^{j(n^-)} \\ +\frac{1}{A_n^+}\overline{\rho}_m^{c-}\cdot\overline{F}_{p(m^-)q(n^+)}^{j(n^+)} - \frac{1}{A_n^-}\overline{\rho}_m^{c-}\cdot\overline{F}_{p(m^-)q(n^-)}^{j(n^-)} \end{array}\right\}$$
$$+\frac{l_m l_n}{\pi j\omega\mu}\left\{\begin{array}{c} \frac{1}{A_n^+}\varphi_{p(m^+)q(n^+)} - \frac{1}{A_n^-}\varphi_{p(m^+)q(n^-)} \\ -\frac{1}{A_n^+}\varphi_{p(m^-)q(n^+)} + \frac{1}{A_n^-}\varphi_{p(m^-)q(n^-)} \end{array}\right\} \quad (9)$$

Here, the subscript $p(m^{\pm})$ denotes the triangle number of either plus or minus triangle associated with mth RWG function. The subscript $q(n^{\pm})$ has a similar meaning. Superscript $j(n^{\pm})$ is the free vertex number of either plus or minus triangle associated with the nth RWG function. Hence, by using this admittance matrix filling approach, possible double calculation of the same surface integral can be avoided.

For plane wave incidence, an element of the excitation vector $\overrightarrow{I}^i$ can be expressed as

$$I_m^i = l_m\left\{\overline{\rho}_m^{c+}\cdot\overline{H}_t^{io}\left(\overline{r}_m^{c+}\right) + \overline{\rho}_m^{c-}\cdot\overline{H}_t^{io}\left(\overline{r}_m^{c-}\right)\right\} \quad (10)$$

where

$$\overline{H}_t^{io}\left(\overline{r}_m^{c\pm}\right) = \left(\hat{u}_\theta H_\theta^i + \hat{u}_\varphi H_\varphi^i\right)e^{-j\overline{k}_i\cdot\overline{r}_m^{c\pm}}$$

$$k_i = -k(\hat{x}\sin\theta_i\cos\varphi_i + \hat{y}\sin\theta_i\sin\varphi_i + \hat{z}\cos\theta_i)$$

By solving (1) for the unknown coefficients, the transmitted power P_{trans} and the far-field magnetic field H_m can be computed. From these quantities, the transmission coefficient, T, and the transmission cross-section, τ, can be determined by following [15] and are given by

$$T = \frac{\frac{1}{2}\mathrm{Re}\left(\widetilde{V}\,\overrightarrow{I}^{i*}\right)}{\eta|H^{io}|^2 A\cos\theta_i} \quad (11)$$

$$\tau = \frac{\omega^2\varepsilon^2}{8\pi}\left|\widetilde{I}^m\overrightarrow{V}\right|^2 / \left|\overline{H}^{io}\right|^2 \quad (12)$$

where A is the total area of the aperture, θ_i is the angle of incidence of the plane wave and η is the intrinsic impedance of the medium.

In this work, the transmission cross-section has been normalized with respect to the first resonant wavelength, λ_1, of fractal geometry and is expressed in dB as

$$\tau(\mathrm{dB}) = 10\log\left(\frac{\tau}{(\lambda_1)^2}\right) \quad (13)$$

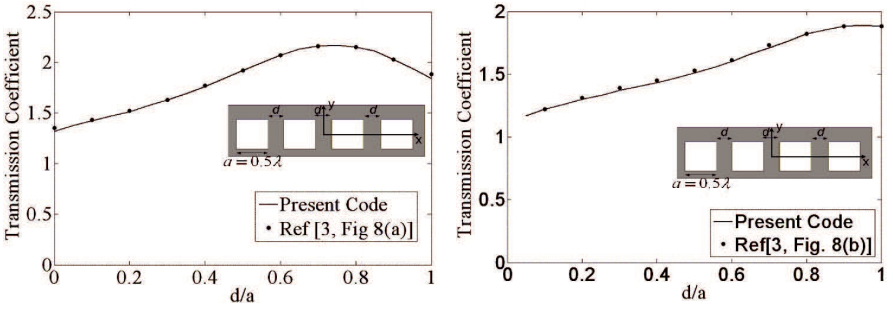

(a) x-polarized incident wave (b) y-polarized incident wave

Figure 4. Transmission coefficient for a row of 4 square apertures versus the spacing between the apertures at normal incidence.

3. NUMERICAL RESULTS

Based on the formulation described in Section 2, a MATLAB code has been developed to find the transmission properties of various fractal apertures. In all the numerical examples, we have considered free space on either side of the screen. In order to verify the accuracy of the developed code, first we have computed the transmission coefficient for a row of four square apertures at normal incidence with different spacing between the apertures. Fig. 4 compares the results obtained from the present analysis with those reported in [3], where an excellent agreement can be seen. Fig. 5 shows the transmission cross section of six apertures for perpendicular polarization with angle of incidence equal to 45°. Again, the results can be seen to agree well with those given in [3, Fig. 14].

3.1. Sierpinski Gasket

Sierpinski gasket [23] can be constructed by subtracting a central inverted triangle from the original triangle. If this process is successively iterated on the remaining triangles, then after an infinite number of iterations, we obtain the ideal Sierpinski gasket fractal. A Sierpinski gasket of 2nd iteration is shown in Fig. 6. Before analyzing the gasket geometry, we first analyzed the transmission characteristics of a single triangular aperture in the conducting screen illuminated by a plane wave at normal incidence. The variation of transmission coefficient for different base width (w) with a fixed height (h) of 120 mm is shown in Fig. 7 for x- and y-polarized incident waves. Since the electric field vector for x-polarized incident wave is perpendicular to

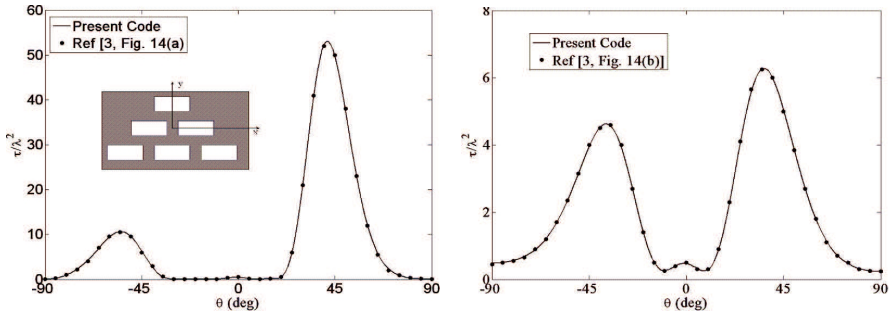

(a) φ = 0° (b) φ = 90°

Figure 5. Transmission cross-section of six rectangular apertures for a plane wave with perpendicular polarization. The angle of incidence is 45°. The dimension of each aperture is $1\lambda \times 0.5\lambda$ and the distance between each aperture is 0.25λ.

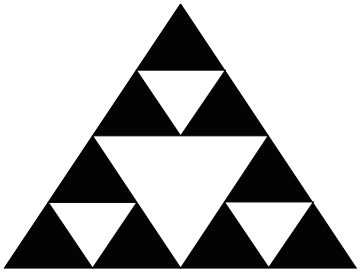

Figure 6. Sierpinski gasket of 2nd iteration.

the height of the triangle, the resonant frequency remains constant with resonant wavelength approximately equal to $2h$. For the y-polarized incident wave, it can be seen from Fig. 7(b) that the resonant frequency shifts downwards as w is increased and for each case, the resonant wavelength is approximately $2w$. Thus, the dimension perpendicular to the electric field determines the resonant frequency of the aperture, a behavior similar to that exhibited by a rectangular aperture. A similar behavior can be seen from Fig. 8, which shows the variation of transmission coefficient for different h, with $w = 120\,\text{mm}$.

The properties of a five iteration Sierpinski monopole antenna have been studied in [24]. It was found that the antenna shows log-periodic behavior with the bands separated by a factor of 2. Also, as the order of iteration is increased, the frequency shifts toward lower frequency region. Here, we have considered a 2nd iterated Sierpinski

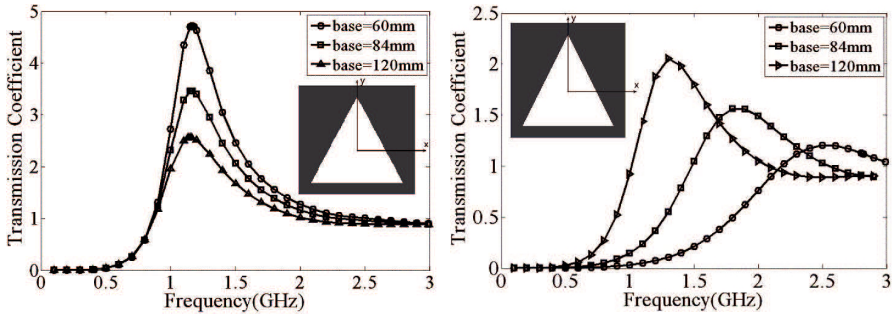

(a) x-polarized incident wave (b) y-polarized incident wave

Figure 7. Transmission coefficient of a triangular aperture of different base width (w) with height (h) = 120 mm.

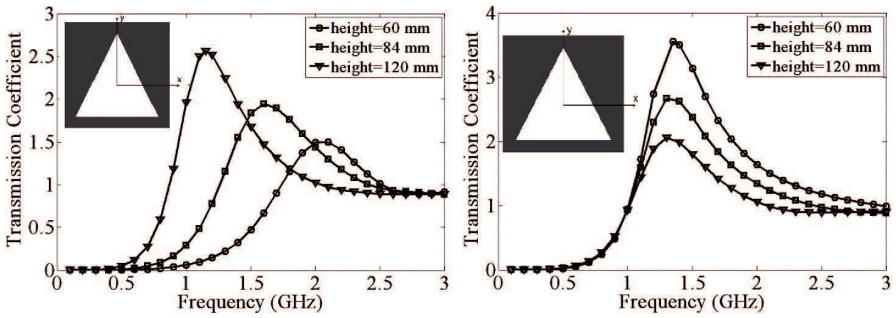

(a) x-polarized incident wave (b) y-polarized incident wave

Figure 8. Transmission coefficient of a triangular aperture of different height (h) with base width (w) = 120 mm.

gasket aperture as shown in Fig. 9 with $h = 88.9$ mm. The transmission coefficients for three different iterations are shown in Fig. 10 for a range of frequencies from 0.1 to 12 GHz. Table 1 summarizes the main performance parameters of the Sierpinski gasket aperture.

It can be seen from the table that, as the order of iteration increases, the resonant frequency shifts downwards. Also, the transmission coefficients at a particular resonant frequency increase with the order of iteration with a low transmission between two pass bands. Hence, the structure exhibits good bandpass characteristics. From a study of the aperture magnetic current distribution, it was found that, as the order of iteration increases, the magnitude of equivalent magnetic surface current increases, which causes the increase in transmission coefficient. In [8], a dual band FSS based

Table 1. Transmission parameters of Sierpinski gasket aperture.

Iteration	*x*-polarized incident wave			*y*-polarization incident wave		
	Resonant Frequency (GHz)	Transmission coefficient	Ratio (f_{n+1}/f_n)	Resonant Frequency (GHz)	Transmission coefficient	Ratio (f_{n+1}/f_n)
0	1.54	2.31	-	1.54	2.31	-
1	1.40	4.05	-	1.37	4.09	-
	4.60	1.49	3.29	4.58	1.49	3.34
2	1.32	7.80	-	1.31	7.78	-
	3.90	3.61	2.95	3.92	3.59	2.99
	8.90	2.09	2.28	8.95	2.08	2.28

on Sierpinski gasket dipole was reported and it was stated that the first two resonant frequency occur at

$$\frac{2h}{\lambda_1} = 0.4 \qquad \frac{2h}{\lambda_2} = 1.13 \tag{14}$$

where λ_1 and λ_2 are the free space wavelength for first two resonant frequencies. According to (14), the first two resonant frequencies for the present geometry should be at 1.35 GHz and 3.81 GHz. From Table 1, it can be seen that the first two resonant frequencies occur at 1.32 GHz and 3.90 GHz which are within 2% of those predicted by (14). Also, the frequency ratios between successive resonant frequencies tend to approach 2, which is the scale factor of gasket geometry, for higher order bands as the number of iterations increases. Since the initial

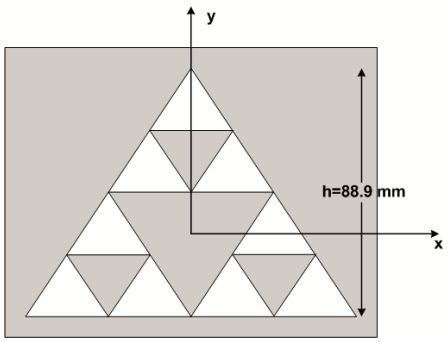

Figure 9. Sierpinski gasket aperture of 2nd iteration in infinite conducting screen. The white portions denote the aperture regions.

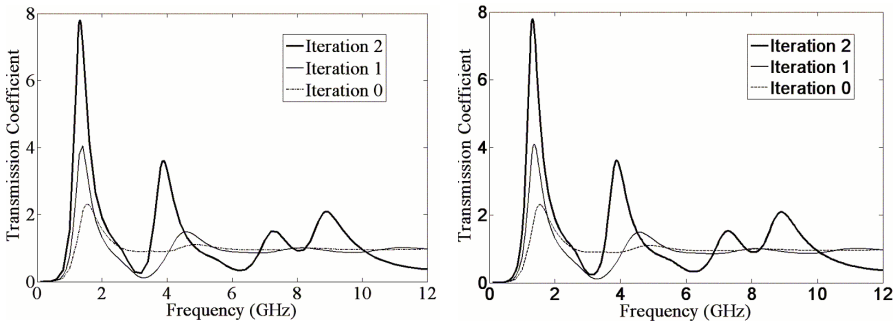

(a) x-polarized incident wave (b) y-polarized incident wave

Figure 10. Transmission coefficient of Sierpinski gasket aperture for different iterations at normal incidence.

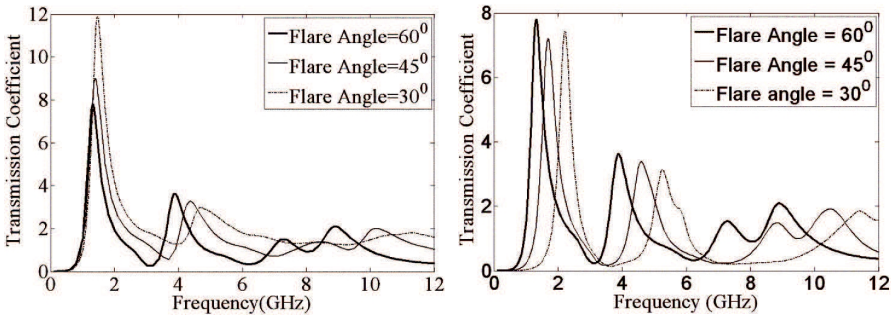

(a) x-polarized incident wave (b) y-polarized incident wave

Figure 11. Variation of transmission coefficient of 2nd iterated Sierpinski gasket aperture for different flare angle at normal incidence.

triangle was an equilateral triangle, the response of the aperture for x- and y-polarized incident wave is almost similar.

Next, the flare angle of the triangle was varied. The transmission characteristics of the gasket aperture for three values of flare angles, $\alpha = 30°$, $\alpha = 45°$ and $\alpha = 60°$ for x- and y-polarized incident waves at normal incidence have been studied and are shown in Fig. 11. It is evident from Fig. 11(a) that, as the flare angle of gasket aperture decreases, the transmission coefficient at the first resonant frequency increases. This is in line with our expectations, since a similar behavior was exhibited by a single aperture (Fig. 7(a)). It may be mentioned here that a similar variation of the resonant frequencies has been seen for a Sierpinski monopole antenna [25]. The transmission coefficient at the second and third resonant frequency decreases with

the decrease in flare angle and the response for a flare angle of 30° becomes almost flat for frequencies greater than 6 GHz. However, as shown in Fig. 11(b), for y-polarized incident wave, the fractal property remains unchanged, with a upward shift of resonant frequency as the flare angle is decreased. It is because, for y-polarized incident wave, the electric field is perpendicular to the base length and a decrease in flare angle means a smaller base length which corresponds to higher resonant frequencies.

The far-field characteristics of the gasket aperture have been expressed in terms of the transmission cross-section. The transmission cross-section patterns of gasket aperture in two principle planes $\phi = 0°$ and $\phi = 90°$ for x- and y-polarized incident wave are shown in Fig. 12. It can be seen from the figures that at higher resonant frequencies, the patterns become more directive and also, side lobes are generated.

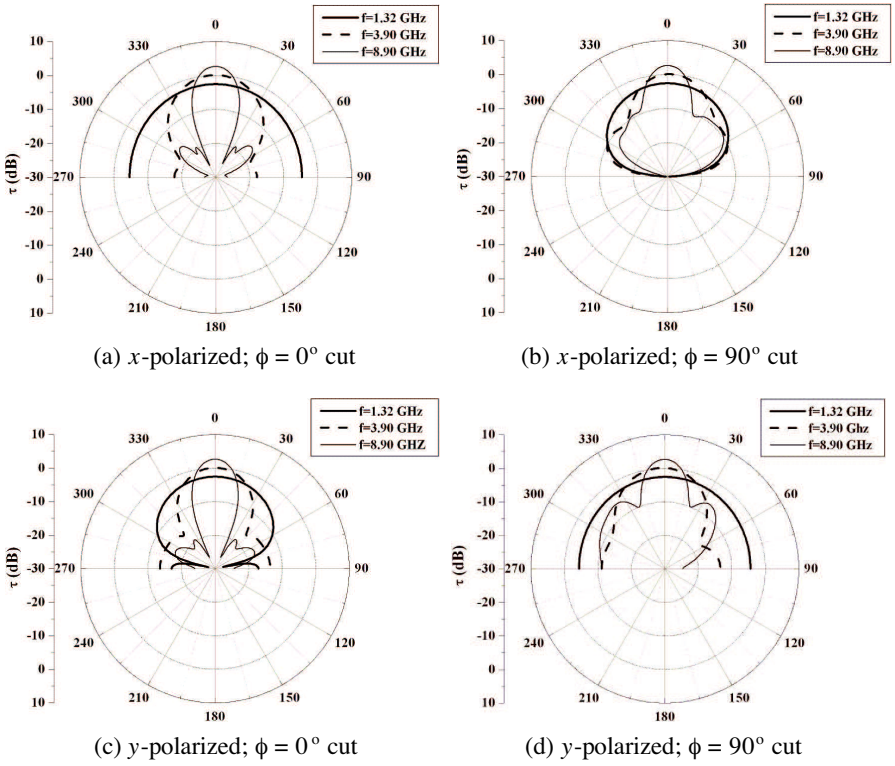

Figure 12. Transmission cross-section patterns of 2nd iterated Sierpinski gasket aperture at three resonant frequencies with normal incidence.

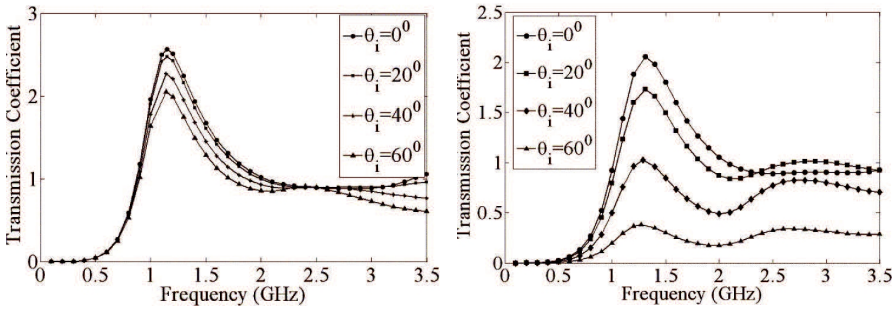

(a) Parallel polarization (b) Perpendicular polarization

Figure 13. Variation of transmission coefficient of a triangular aperture for different angles of incidence.

Next, in order to find out the behavior of the aperture for different incidence angle, the angle of incidence was varied. In this case, the transmission coefficient is normalized with respect to the incident power density at normal incidence rather than the actual power density at oblique incidence. First, the behavior of a single triangular aperture of dimension $w = 120\,\text{mm}$ and $h = 120\,\text{mm}$ was analyzed for different angles of incidence for both parallel and perpendicular polarizations. The variation of transmission coefficient for different angles of incidence are shown in Fig. 13. As the angle of incidence is increased, for parallel polarization, a weak second resonance is generated around 2.4 GHz corresponding to $\frac{h}{\lambda} = 0.96$. On the other hand, the second resonance appears around 2.8 GHz for perpendicularly polarized incident wave which gives $\frac{w}{\lambda} = 1.12$. Also, the value of transmission coefficient decreases as the angle of incidence is increased and this decrement is sharper for perpendicular polarization. In order to get an insight into this phenomenon, we have plotted the surface current distribution over the triangular aperture. The plots of magnitude and phase of y-component of current along $y = -31.25$ cut for parallel polarization at 1.15 GHz and 2.4 GHz are shown in Fig. 14. It can be seen from the current distribution that, at the primary resonant frequency of the triangular aperture, the magnitude and phase of M_y is almost uniform over the entire width of the triangle. Also, it is evident that the magnitude of the current changes very little with the change in angle of incidence at primary resonance. At the second resonance, the current distribution shows a nearly uniform phase distribution for normal incidence. However, as the angle of incidence is varied, the phase of M_y changes around the center line of the triangle which causes a resonance. The magnitude of current is well below the magnitude at primary

resonance which causes a weak response. Similar behavior is obtained for perpendicular polarization as seen from Fig. 15. As the angle of incidence is increased, the magnitude of current decreases sharply for perpendicular polarization as compared to parallel polarization, which causes a sharp decrease in the value of transmission coefficient at oblique incidence for perpendicular polarization.

Now, the angle of incidence is varied for a 2nd iterated Sierpinski gasket aperture. The variations of transmission coefficient for different incidence angle for both polarizations are shown in Fig. 16. It is found that, in addition to the three resonant frequencies as given in Table 1, two more resonant frequencies appear around 2.80 GHz and 5.95 GHz for parallel polarization and around 2.75 GHz and 6.00 GHz for perpendicular polarization as shown in Table 2 and Table 3. These additional resonant wavelengths are around 1λ as was the case from single aperture. The behavior of current at those additional resonant frequencies are expected to be same as that of single triangular aperture.

Table 2. Transmission parameters of Sierpinski gasket aperture for different angle of incidence with parallel polarization.

θ_i	f_1	f_2	f_3	f_4	f_5	h_1/λ_2	h_2/λ_4
0	1.32	-	3.88	-	8.90	-	-
20	1.32	-	3.88	-	8.90	-	-
40	1.31	2.81	3.84	5.98	8.01	0.83	0.89
60	1.31	2.80	3.76	5.97	7.29	0.83	0.88

Table 3. Transmission parameters of Sierpinski gasket aperture for different angle of incidence with perpendicular polarization.

θ_i	f_1	f_2	f_3	f_4	f_5	h_1/λ_2	h_2/λ_4
0	1.32	-	3.88	-	8.95	-	-
20	1.32	2.75	3.88	5.78	8.18	0.94	0.99
40	1.31	2.78	3.92	5.80	8.81	0.95	0.99
60	1.31	2.78	4.24	5.99	8.71	0.95	1.03

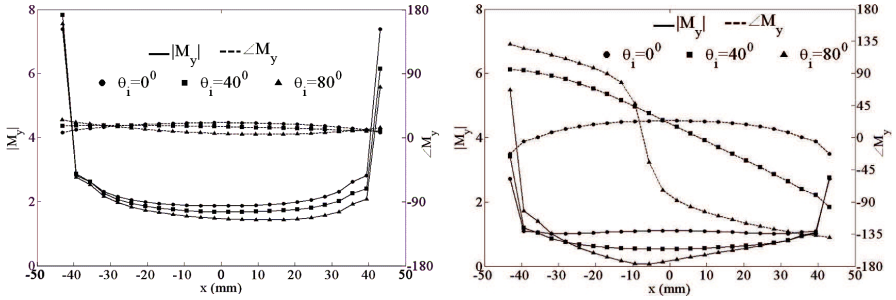

(a) Primary resonance at $f = 1.15$ GHz (b) Secondary resonance at $f = 2.4$ GHz

Figure 14. Variation of current distribution of a triangular aperture with different angles of incidence at primary and secondary resonances with parallel polarization.

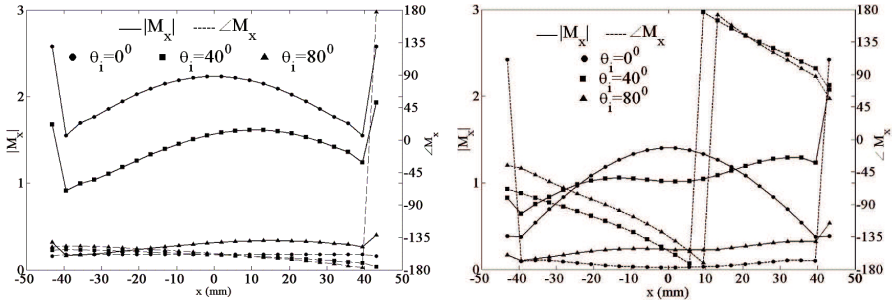

(a) Primary resonance at $f = 1.30$ GHz (b) Secondary resonance at $f = 2.8$ GHz

Figure 15. Variation of current distribution of a triangular aperture with different angle of incidence at primary and secondary resonances with perpendicular polarization.

3.2. Koch Curve

Koch curve monopole and dipole antennas have multiband property and are widely used in antenna miniaturization. In [26], a multi-resonant dipole antenna based on Koch curve has been studied. It has been shown that by changing the indentation angle of the curve, which in turn changes the fractal dimension, the input characteristics of the Koch antennas can be changed. Iterated Function System (IFS) for a generalized Koch curve with a scale factor s and indentation angle

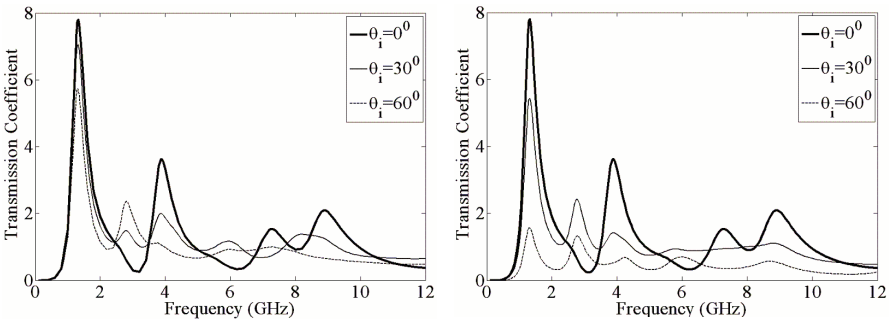

(a) Parallel polarization (b) Perpendicular polarization

Figure 16. Variation of transmission coefficient of 2nd iterated Sierpinski gasket aperture for different angles of incidence.

θ can be expressed as [26],

$$W_1 \begin{pmatrix} x \\ y \end{pmatrix} = \begin{pmatrix} \frac{1}{s} & 0 \\ 0 & \frac{1}{s} \end{pmatrix} \begin{pmatrix} x' \\ y' \end{pmatrix} \tag{15}$$

$$W_2 \begin{pmatrix} x \\ y \end{pmatrix} = \begin{pmatrix} \frac{1}{s}\cos\theta & -\frac{1}{s}\sin\theta \\ \frac{1}{s}\sin\theta & \frac{1}{s}\cos\theta \end{pmatrix} \begin{pmatrix} x' \\ y' \end{pmatrix} + \begin{pmatrix} \frac{1}{s} \\ 0 \end{pmatrix} \tag{16}$$

$$W_3 \begin{pmatrix} x \\ y \end{pmatrix} = \begin{pmatrix} \frac{1}{s}\cos\theta & \frac{1}{s}\sin\theta \\ -\frac{1}{s}\sin\theta & \frac{1}{s}\cos\theta \end{pmatrix} \begin{pmatrix} x' \\ y' \end{pmatrix} + \begin{pmatrix} \frac{1}{2} \\ \frac{1}{s}\sin\theta \end{pmatrix} \tag{17}$$

$$W_4 \begin{pmatrix} x \\ y \end{pmatrix} = \begin{pmatrix} \frac{1}{s} & 0 \\ 0 & \frac{1}{s} \end{pmatrix} \begin{pmatrix} x' \\ y' \end{pmatrix} + \begin{pmatrix} \frac{s-1}{s} \\ 0 \end{pmatrix} \tag{18}$$

where

$$s = 2(1 + \cos(\theta)) \tag{19}$$

The self-similarity dimension of the curve is given by

$$D = \frac{\log 4}{\log s} \tag{20}$$

Hence, by changing the indentation angle, we can change the fractal dimension. Generalized Koch curve geometries for two indentation angles are shown in Fig. 17.

Here, we have investigated the transmission properties of the Koch fractal slot of varying fractal dimension in an infinite conducting

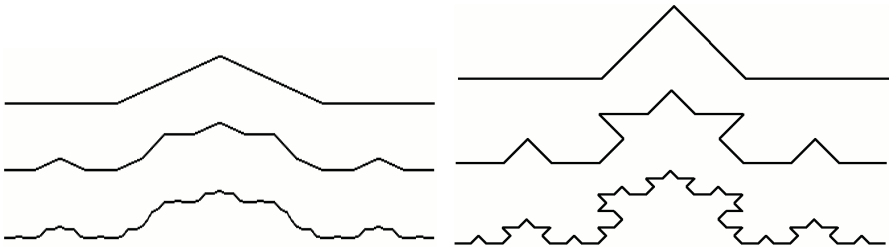

(a) Indentation angle = 20 ° (b) Indentation angle = 60 °

Figure 17. Koch curve with different indentation angles.

screen illuminated by a plane wave. For the present analysis, we have considered a rectangular slot of length 20 cm along the x-axis and width 5 mm along the y-axis as the initiator. A y-polarized wave is assumed to be normally incident on the Koch slot. Fig. 18 shows the transmission coefficients of a Koch slot of 60° indentation angle for three different iterations. It can be seen that the resonant frequencies reduce as the order of iteration is increased. This is expected, since the total length of the slot increases with the order of iteration although the end-to-end length remains constant at 20 cm. Another factor that has a strong influence on the value of the resonant frequencies and the magnitude of transmission coefficient at resonance, is the indentation angle. The variation of the primary resonant frequency (f_{r1}) for the first three iterations is given in Table 4 and the variation

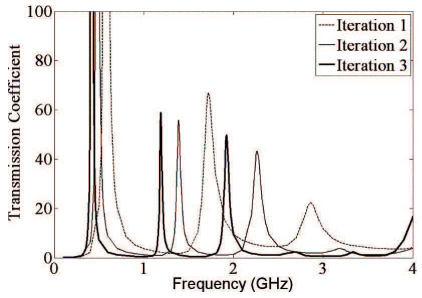

Figure 18. Transmission coefficient of Koch fractal slot for different iterations with 60° indentation angle.

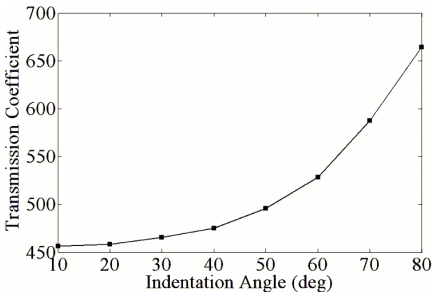

Figure 19. Variation of transmission coefficient with different indentation angle at primary resonant frequency of Koch fractal slot of 3rd iteration.

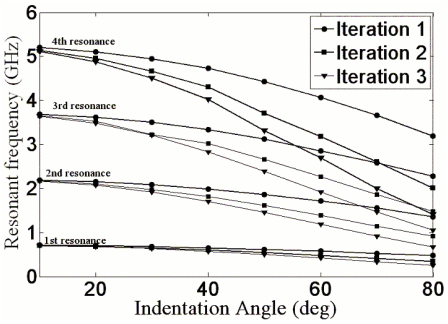

Figure 20. Variation of resonant frequencies with different indentation angle for Koch fractal slot.

of magnitude of transmission coefficient at f_{r1} for different indentation angle is shown in Fig. 19, for a 3rd iterated Koch slot. From a study of surface current distribution of Koch slot at the primary resonance, it is found that the current is maximum at the center of the slot and the magnitude of the maxima increases with the increase in indentation angle, which causes the increase in transmission coefficient. Thus, the indentation angle can be made a design parameter in order to achieve a good transmission property at a particular frequency. The variations of resonant frequencies for three iterations with different indentation angles are shown in Fig. 20. It may be noted that the higher order resonant frequencies shift by larger amount than the lower order resonant frequencies. The ratio between successive resonant frequencies also changes with the change in indentation angle. The ratios of successive resonant frequencies with the indentation angle are tabulated in Table 5 from which it is evident that the indentation angle can be varied in order to place the transmission bands at desired locations. It is evident that the ratios are different for each interval, but they remain nearly constant for different iterations of the same dimension. It may be mentioned here that a Koch fractal slot is expected to have characteristics similar to those of Koch monopole. The results presented here agree very well with those presented in [26] for a Koch dipole antenna.

The transmission cross-section of a third iteration standard Koch slot for two orthogonal planes is shown in Fig. 21. It should be noted that the transmission cross-section at the resonant frequencies are similar to that of a linear slot. As the frequency is increased, some ripples are found in the transmission cross-section pattern. Also, it may be noticed that the transmission cross-section patterns remain almost symmetric for both the planes.

Table 4. Variation of f_{r1} for Koch aperture with indentation angle.

Indentation Angle (deg)	First Resonant frequency for various iterations of Koch slot (GHz)		
	Iteration 1	Iteration 2	Iteration 3
10	0.710	0.707	0.706
20	0.698	0.686	0.678
30	0.678	0.651	0.633
40	0.651	0.604	0.573
50	0.618	0.547	0.500
60	0.577	0.482	0.420
70	0.529	0.410	0.335
80	0.484	0.342	0.258

Next, the angle of incidence was varied for a Koch curve of 3rd iteration with 60° indentation angle. The normalized transmission coefficient for different angle of incidence for a perpendicularly polarized incident wave is shown in Fig. 22. It can be seen that, similar to gasket apertures, the variation of incidence angle introduces additional resonant frequencies around 814 MHz and 1580 MHz. As the angle of incidence is increased, the transmission coefficient at the resonant frequencies for normal incidence decreases and for $\theta_i = 60°$,

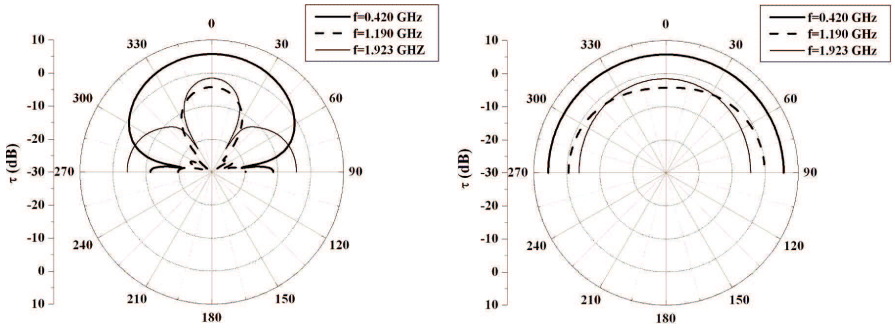

Figure 21. Transmission cross-section pattern of 3rd iterated Koch fractal slot with indentation angle equal to 60°.

Table 5. Ratios between successive resonant frequencies of generalized Koch slot.

Indentation Angle	Fractal Dimension	Fractal Iteration	f_2/f_1	f_3/f_2	f_4/f_3
10	1.006	1	3.09	1.68	1.41
		2	3.08	1.68	1.40
		3	3.08	1.68	1.40
20	1.023	1	3.08	1.68	1.41
		2	3.06	1.68	1.40
		3	3.06	1.68	1.40
30	1.053	1	3.07	1.68	1.41
		2	3.04	1.63	1.44
		3	3.03	1.67	1.40
40	1.099	1	3.05	1.68	1.42
		2	3.00	1.67	1.42
		3	2.98	1.65	1.42
50	1.165	1	3.02	1.67	1.42
		2	2.95	1.65	1.40
		3	2.92	1.63	1.39
60	1.262	1	2.98	1.66	1.42
		2	2.88	1.63	1.41
		3	2.83	1.62	1.40
70	1.404	1	2.94	1.66	1.42
		2	2.79	1.63	1.40
		3	2.73	1.60	1.36
80	1.625	1	2.81	1.68	1.40
		2	2.67	1.62	1.36
		3	2.59	1.58	1.34

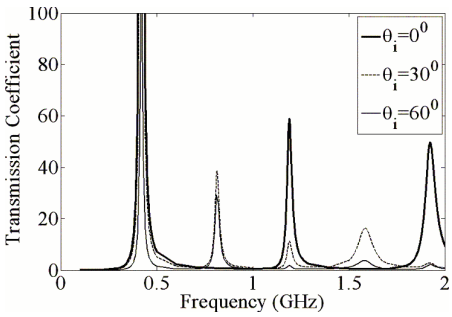

Figure 22. Variation of transmission coefficient with different angle of incidence for 3rd iterated Koch fractal slot with indentation angle is 60°.

the response becomes almost flat for frequencies greater than 1 GHz. Although, the transmission coefficient at the new resonant frequencies increases with increase in angle of incidence up to around 40°, it again decreases with increase in θ_i beyond 40°. To understand this phenomena, we studied the magnetic current distribution of a rectangular slot. It was found that, similar to the behavior obtained for a triangular aperture, an additional weak secondary resonance appears around $L = \lambda$ for inclined incidence, where L is the length of the slot. Also, the phase of the dominant component of current undergoes a phase reversal at the secondary resonant frequency, a behavior similar to that of the triangular aperture. The magnitude of current shows two maxima which are $L/2$ distance apart. The same behavior was seen in case of Koch curve for oblique incidence.

3.3. Hilbert Curve

Due to their space filling properties, the Hilbert curve can enclose longer curves in a given area than the Koch curve; hence it has been used for further miniaturization of monopole and dipole antennas [27]. The self-similarity of this geometry leads to a multi-band operation. The topological dimension of Hilbert curve is 1, since it is a simple curve. But, for a large number of iterations, the fractal dimension of the curve approaches 2. Considering the length and number of line segments in first and second iterations, the fractal dimension is 1.465. The corresponding fractal dimensions for next two iterations are 1.694 and 1.834, respectively. A fourth iterated Hilbert curve is shown in Fig. 23. In our analysis, the Hilbert geometry is assumed to occupy an area of 7.5 cm × 7.5 cm with the width of the slot taken to be 1 mm.

The transmission characteristics of different iterations of Hilbert curve fractal aperture illuminated by a plane wave of x- and y-polarizations with normal incidence are shown in Fig. 24. The difference in the transmission coefficient plots for x- and y-polarization is due to the fact that the curve is symmetric with respect to y-axis but asymmetric with respect to x-axis. It can be seen from the plot that the Hilbert aperture offers a multi-band behavior and the resonant frequencies decrease as the order of iteration increases due to the increase in the length of the slot. The variation of first resonant frequency for different iterations of Hilbert curve aperture is summarized in Table 6. The transmission bandwidth increases for higher order resonances, whereas, it decreases significantly as the order of iteration increases. Since the transmission coefficient plots show sharp transmission bands with very low transmission between two resonant peaks, it offers excellent band stop characteristics. Again from the current distribution plots, it was found that the current is distributed over the entire aperture region and at the higher resonances, the current is concentrated in the scaled copies of the geometry. Also, the magnitude of surface current decreases with increase in order of resonance which causes the decreases in transmission coefficient.

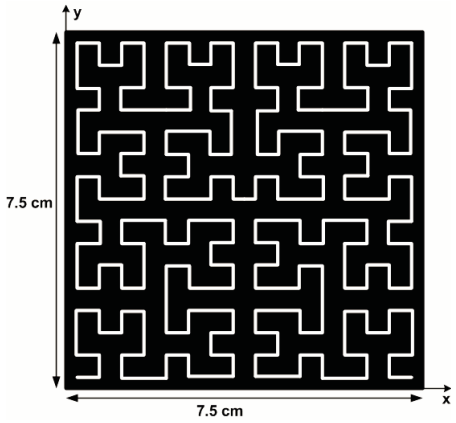

Figure 23. Hilbert fractal slot of 4th iteration.

The transmission cross-section patterns for a 4th iterated Hilbert aperture at its first four resonant frequencies are shown in Fig. 25. From the transmission cross-section plots for both x- and y-polarizations, it may be stated that the pattern are symmetric at all resonant frequencies, although, the patterns get narrower for higher order resonant frequencies.

The variation of transmission coefficient of a 4th iterated Hilbert

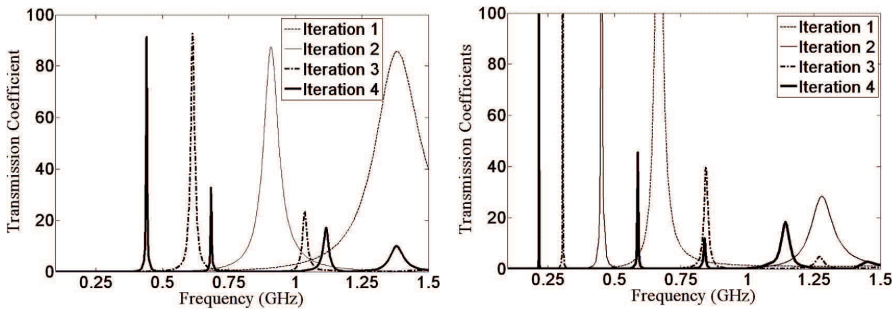

(a) x-polarized incident wave (b) y-polarized incident wave

Figure 24. Transmission coefficient of Hilbert slot for different iterations at normal incidence.

Table 6. Primary resonant frequency of Hilbert curve aperture of different iteration

Iteration	Primary resonant frequency (GHz)	
	x-polarized	y-polarized
1	1.383	0.666
2	0.908	0.452
3	0.614	0.306
4	0.440.4	0.2172

aperture with angle of incidence is shown in Fig. 26. Again, some additional resonances occur as the angle of incidence is increased. The transmission coefficients at these additional resonant frequencies increase with the increase in angle of incidence. The occurrence of these resonance can again be explained in similar manner as in Koch slot from the current distribution which shows additional maxima at inclined incidence. For perpendicular polarization, some additional resonant frequencies appear but, the transmission coefficients at these frequencies are very small as compared to those at the resonant frequencies for normal incidence. Also, the transmission coefficient at a particular resonant frequency decreases with increase in angle of incidence and the decrease is sharper in case of perpendicular polarization.

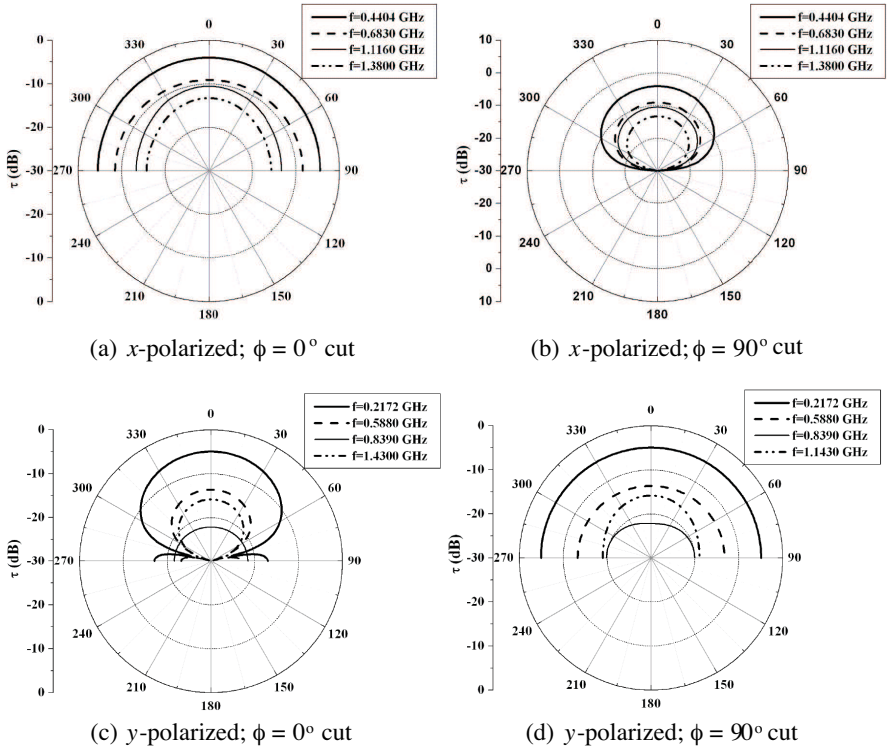

(a) x-polarized; $\phi = 0^{\circ}$ cut (b) x-polarized; $\phi = 90^{\circ}$ cut

(c) y-polarized; $\phi = 0^{\circ}$ cut (d) y-polarized; $\phi = 90^{\circ}$ cut

Figure 25. Transmission cross-section pattern of 4th iterated Hilbert slot at the first four resonant frequencies.

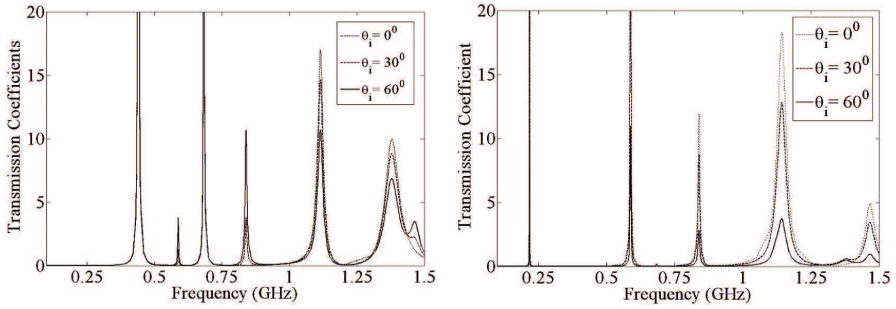

(a) Parallel polarization (b) Perpendicular polarization

Figure 26. Variation of transmission coefficient with different angle of incidence of 4th iterated Hilbert slot.

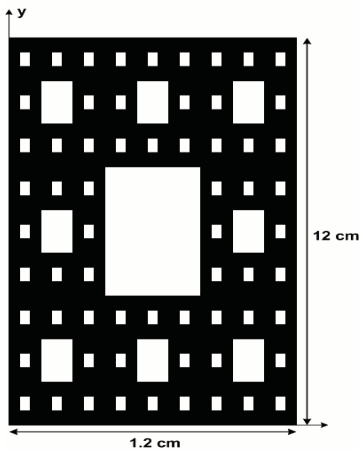

Figure 27. Sierpinski carpet aperture of 3rd iteration.

3.4. Sierpinski Carpet

Another fractal that can be used in multi-band antennas and FSS is Sierpinski carpet fractal [9]. The geometry of a third iterated Sierpinski carpet structure is shown in Fig. 27. The dimension used in the present analysis has an initial rectangular geometry of dimensions $1.2\,\text{cm} \times 12\,\text{cm}$. The transmission characteristics of different iterations of the fractal aperture for x-polarized incident wave at normal incidence are shown in Fig. 28. Again, it can be noted from the plots that the resonant frequency decreases as the order of iteration increases. Basically, the first iteration consists of a single aperture of dimension $0.4\,\text{cm} \times 4\,\text{cm}$ with the larger dimension along y direction. The first resonance occurs at a frequency of 3.30 GHz whose corresponding wavelength is twice the length of the slot in y-direction. In the next iteration, the aperture dimension gets reduced by a factor 3, and hence it is expected to have the second resonant frequency which is three times the first resonant frequency. Thus, the ratio between the successive resonant frequencies is approximately 3. For a 3rd iteration Sierpinski carpet aperture the resonant frequencies occurs at 3.3 GHz, 10.4 GHz and 33.7 GHz with frequency ratios as $f_2/f_1 = 3.15$ and $f_3/f_2 = 3.24$. Hence, the resonant frequencies are separated by a factor approximately equal to the theoretical value 3.

The transmission cross-section patterns of 3rd iterated Sierpinski carpet fractal aperture for x-polarized incident wave in two orthogonal planes are shown in Fig. 29. It can be seen from the plots that the maximum value of transmission cross section increases for higher order

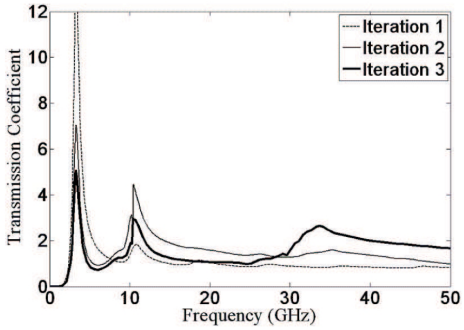

Figure 28. Variation of transmission coefficient for Sierpinski carpet aperture with different iterations.

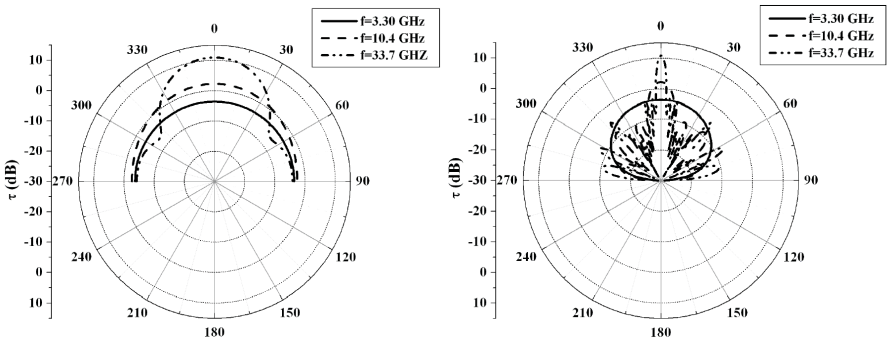

(a) $\phi = 0^o$ (b) $\phi = 90^o$

Figure 29. Transmission cross-section of 3rd iteration Sierpinski carpet aperture at first three resonant frequencies.

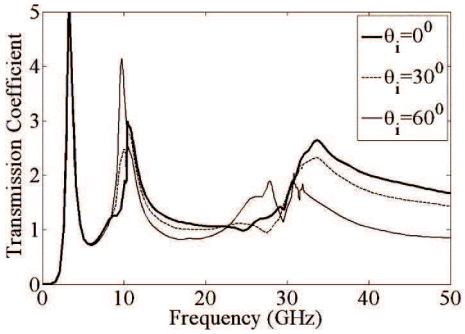

Figure 30. Variation of transmission coefficient with different angle of incidence for 3*rd* iterated Sierpinski carpet aperture.

resonant frequencies. Also, for $\varphi = 90°$ plane, a large number of side lobes are generated for third resonant frequency.

The effect of variation of incidence angle for parallel polarization on the behavior of Sierpinski carpet aperture is shown in Fig. 30. It can be seen from the plot that as the incidence angle is increased, the third resonance peak gets distorted and some spurious peaks arise around 30 GHz.

3.5. Minkowski Curve

Taking a line segment of length L, Minkowski operator divides the line into three equal segments with the middle section having a depth of aL [28]. The coefficient 'a' is known as "depression coefficient". The value of 'a' can be any value between 0 and 1/3 for a square initiator. The Minkowski fractal generator is shown in Fig. 31. In the first iteration, each line segment of the initial square is replaced by the generator curve. This process is successively applied to each line segment in the next iteration step. The Minkowski fractal geometry after second iteration with different values of 'a' are shown in Fig. 32. The variation of transmission coefficient for two iterations of Minkowski fractal aperture with different values of 'a' for x-polarized incident wave at normal incidence are shown in Fig. 33. Since the geometry is symmetric along both x- and y-directions, the transmission characteristics are almost similar for both x- and y-polarized incident wave. For $a = 0.3$, the resonances occur at 0.92 GHz, 3.16 GHz and 12.1 GHz with the ratios between successive resonant frequencies of 3.43 and 3.83, although the third resonance peak is very small as compared to the first two resonant peaks. From the plot, it is evident that the fractal aperture shows a multi-band property for higher values of 'a'. As the value of depression coefficient decreases, the transmission coefficient at a particular resonant frequency decreases, and the higher-order resonant properties diminish. Also, it can be seen from the plot that, as the value of depression coefficient increases, the resonant frequency moves downwards, a behavior similar to that demonstrated in [28] for a Minkowski fractal patch antenna.

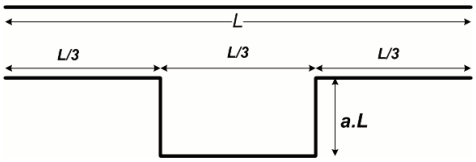

Figure 31. Minkowski fractal generator.

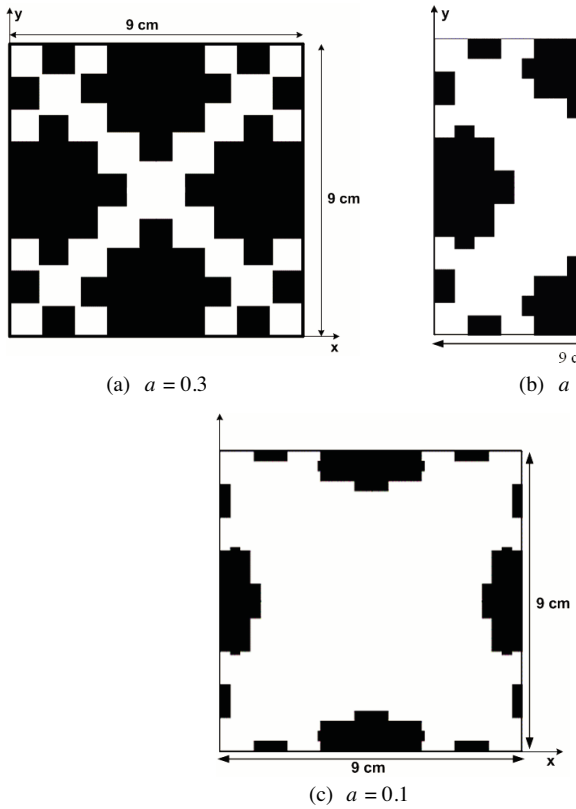

Figure 32. Minkowski fractal geometries after second iteration for different values of depression coefficients.

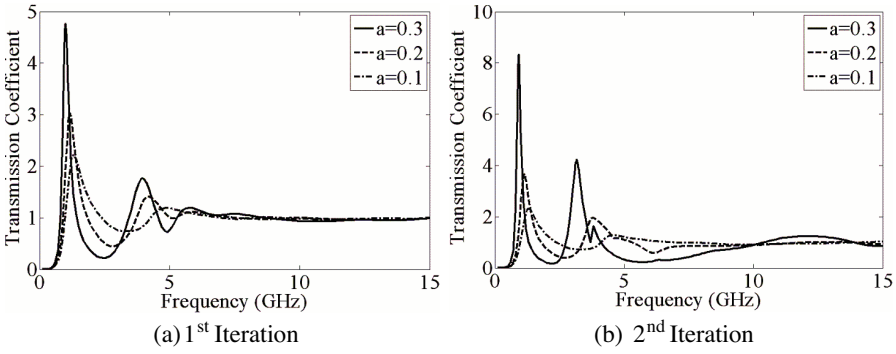

Figure 33. Transmission coefficient of Minkowski fractal aperture for two iterations with different depression coefficients for x-polarized incident wave at normal incidence.

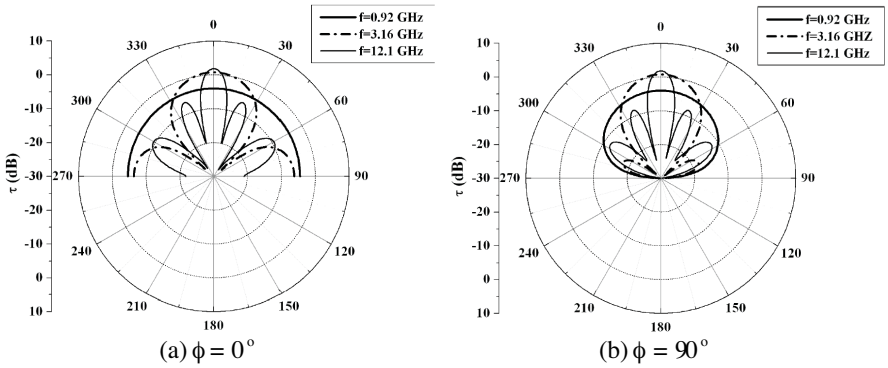

Figure 34. Transmission cross-section of 2nd iterated Minkowski fractal aperture at three resonant frequencies with $a = 0.3$ for x-polarized incident wave at normal incidence.

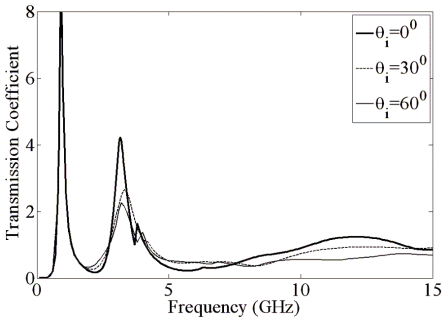

Figure 35. Variation of transmission coefficient with different angle of incidence for 2nd iterated Minkowski aperture.

The transmission cross-section of second iterated Minkowski fractal aperture for $a = 0.3$ with x-polarized incident wave is shown in Fig. 34. It can be seen from the transmission cross-section patterns that the value of transmission cross-section increases for higher resonant frequencies, but the number of side lobes also increases at higher order resonances. Since the geometry is symmetric in x- and y-plane, the cross-section patterns are also symmetric.

The variation of transmission coefficient for different angle of incidence with $a = 0.3$ is shown in Fig. 35. The transmission coefficients at first and second resonant frequencies get reduced with increase in angle of incidence and for higher angles of incidence, the third resonances almost vanishes and hence, the multiband property of fractal is lost.

4. CONCLUSION

Numerical results for a number of fractal shaped apertures in an infinite conducting screen illuminated by a plane wave have been presented which show the existence of multiple passbands. For a Sierpinski fractal aperture, the bands are separated by a factor 2, which is similar to that obtained for a Sierpinski monopole antenna. As long as the initial triangle is equilateral, the transmission characteristics are similar for x- and y-polarized incident wave. Also, it has been found that the fractal property of the gasket aperture depends on the flare angle of the triangle as well as on the polarization of incident wave. The band separation also changes at oblique incidence due to the generation of some new passbands. Also, it is evident form the results that the number of passbands equals the number of iterations for Sierpinski carpet aperture. However, for Sierpinski gasket aperture, a transmission band is obtained for the initial triangular geometry and for any number of iterations, say k, the number of passbands are always $(k + 1)$, as was in case of fractal multiband antenna and FSS. Also, it is true for each fractal geometry that the log periodic behavior can be achieved by using a large number of iterations and since here, we are considering the prefractal geometries, the behavior is quasi log periodic.

Similar to that of a Koch fractal monopole antenna, the Koch fractal slot also possesses multiband characteristics and the location of different passbands can be changed by changing the indentation angle. Hilbert curve fractal slots are very efficient for the reduction of resonant frequency, although the bandwidth of passbands decreases significantly for higher iterations. It has been found that some new passbands occur with the increase in angle of incidence for parallel polarization, whereas, the transmission coefficient at the resonant frequencies decreases significantly with increase in angle of incidence for perpendicular polarization. It may be noted that the Hilbert curve fractal geometry is not strictly self-similar as pointed out in [27], because additional line segments are required to connect the four scaled and rotated copies. However, the lengths of these additional line segments are small as compared to the overall length of the fractal, especially when the order of iteration is very large, which makes the geometry self-similar. For larger order iterations, the self-similarity dimension of the fractal approaches 2 which makes it a true space-filling curve. For lower order iterations, the self-similarity dimension of the fractal geometry can be much less than 2 [27].

The Sierpinski carpet fractal aperture also offers multiple passbands with the passbands separated by a factor of 3, equal to

the self-similarity factor of the geometry. Also, it has been found that the variation of incidence angle does not change the transmission characteristics for lower frequencies, but the third resonance gets distorted. Lastly, it has been shown that the characteristics of Minkowski fractal depend upon the depression coefficient of the Minkowski operator. The transmission coefficient decreases with the increase in angle of incidence, although the ratios of successive bands remain same.

It must also be added here that that the fractals having space-filling properties give rise to enhanced subwavelength transmission as was seen in [11–14]. For example, the lowest frequency of Hilbert curve aperture is 0.2171 GHz for a y-polarized incident wave, corresponding to a wavelength of 138.12 cm which is many times the lateral dimension of the square which it fills. Since the geometry is not symmetric in both planes, the response of the aperture are different for different polarizations as was also seen in case of H shaped fractal slit [14]. The existence of subwavelength transmission can also be found in Koch curve due to their frequency reduction capability. Koch slot was found to have resonant frequencies of 0.484 GHz and 0.577 GHz for indentation angles of 80° and 60°, respectively. The corresponding wavelengths are 61.98 cm and 51.99 cm which are much larger than the Koch curve length. Since, the increase in indentation angle causes the resonant frequency to shift downward and also, the magnitude of transmission coefficient increases, it can be said that at higher indentation angle there is a more enhanced subwavelength transmission. For Minkowski fractal aperture, the lowest resonant frequency is 0.92 GHz for a 2nd iterated fractal with $a = 0.3$, corresponding to a wavelength of 32.6 cm. Again the wavelength is much larger than the lateral dimension of fractal geometry.

On the other hand, self similar structures like Sierpinski gasket and Sierpinski carpet do not exhibit subwavelength transmission, since for these structures the reduction in the first resonance frequency is very small for higher order iterations.

REFERENCES

1. Rahmat-Samii, Y. and R. Mittra, "Electromagnetic coupling through small apertures in a conducting screen," *IEEE Trans. Antennas Propagat.*, Vol. 25, 180–187, Mar. 1977.
2. Sarkar, T. K., M. F. Costa, I. Chin-Lin, and R. F. Harrington, "Electromagnetic transmission through mesh covered apertures and aperture arrays of apertures in a conducting screen," *IEEE Trans. Antennas Propagat.*, Vol. 32, 908–913, Sept. 1984.

3. Andersson, T., "Moment-Method calculations on apertures using basis singular function," *IEEE Trans. Antennas Propagat.*, Vol. 41, 1709–1716, Dec. 1993.
4. Park, H. and H. J. Eom, "Electromagnetic scattering from multiple rectangular apertures in a thick conducting screen," *IEEE Trans. Antennas Propagat.*, Vol. 47, No. 6, 1056–1060, June 1999.
5. Park, Y. B. and H. J. Eom, "Electromagnetic transmission through multiple circular apertures in a thick conducting plane," *IEEE Trans. Antennas Propagat.*, Vol. 52, No. 4, 1049–1055, Apr. 2004.
6. Chen, C. C., "Transmission of microwave through perforated flat plates of finite thickness," *IEEE Trans. Microwave Theory Tech.*, Vol. 21, 1–6, Jan. 1973.
7. Werner, D. H. and R. Mittra (eds.), *Frontiers in Electromagnetics*, Chapter 1–3, Piscataway, NJ, IEEE Press, 2000.
8. Romeu, J. and Y. Rahmat-Samii, "Fractal FSS: A novel dual-band frequency selective surface," *IEEE Trans. Antennas Propagat.*, Vol. 48, 1097–1105, July 2000
9. Gianvittorio, J. P., J. Romeu, S. Blanch, and Y. Rahmat-Samii, "Self-similar prefractal frequency selective surfaces for multiband and dual polarized applications," *IEEE Trans. Antennas Propagat.*, Vol. 51, 3088–3096, Nov. 2003.
10. McVay, J., N. Engheta, and A. Hoorfar, "High impedance metamaterial surfaces using Hilbert curve inclusions," *IEEE Microwave and Wireless Components Letters*, Vol. 14, 130–132, Mar. 2004.
11. Wen, W., L. Zhou, J. Li, W. Ge, C. T. Chan and P. Sheng, "Subwavelength photonic band gaps from planar fractals," *Physical Review Lett.*, vol. 89, No. 22, 223901, Nov. 2002.
12. Zhou, L., C. T. Chan, and P. Sheng, "Theoritical studies on the transmission and reflection properties of metallic planar fractals," *J. Phys. D: Applied Phys.*, Vol. 37, 368–373, 2004.
13. Hou, B., G. Xu, and W. Wen, "Tunable band gap properties of planar metallic fractals," *J. Appl. Phys.*, Vol. 95, No. 6, 3231–3233, Mar. 2004.
14. Wen, W., L. Zhou, B. Hou, C. T. Chan, and P. Sheng, "Resonant transmission of microwaves through subwavelength fractal slits in a metallic plate," *Physical Review B72*, 153406, 2005.
15. Harrington, R. F. and J. R. Mautz, "A generalized network formulation for aperture problems," *IEEE Trans. Antennas*

Propagat., Vol. 24, 870–873, Nov. 1976.

16. Rao, S. M., D. R. Wilton, and A. W. Glisson, "Electromagnetic scattering by surfaces of arbitrary shape," *IEEE Trans. Antennas Propagat.*, Vol. 30, 409–418, May 1982.
17. Chin-Lin, I. and R. F. Harrington, "Electromagnetic transmission through an aperture of arbitrary shape in a conducting screen," Tech Rep-82-5 on Contract N00014-76-C-0025, Syracuse Univ., Apr. 1982.
18. Wilton, D. R., S. M. Rao, A. W. Glisson, D. H. Schaubert, O. M. Al-Bundak, and C. M. Butler, "Potential integrals for uniform and linear source distributions on polygonal and polyhedral domains," *IEEE Trans. Antennas Propagat.*, Vol. 32, 276–281, Mar. 1984.
19. Graglia, R. D., "On the numerical integration of the linear shape functions times the 3D Green's function or its gradient on a plane triangle," *IEEE Trans. Antennas Propagat.*, Vol. 41, 1448–1455, Oct. 1993.
20. Eibert, T. F. and V. Hansen, "On the calculation of potential integrals for linear source distributions on triangular domains," *IEEE Trans. Antennas Propagat.*, Vol. 43, 1499–1502, Dec. 1995.
21. Rossi, L. and P. J. Cullen, "On the fully numerical evaluation of the linear shape function times 3D Green's function on a plane triangle," *IEEE Trans. Microwave Theory Tech.*, Vol. 47, 398–402, Apr. 1999.
22. Khayat, M. A. and D. R. Wilton, "Numerical evaluation of singular and near-singular potential integrals," *IEEE Trans. Antennas Propagat.*, Vol. 53, 3180–3190, Oct. 2005.
23. Peitgen, H. O., H. Jurgens, and D. Saupe, *Chaos and Fractals, New Frontiers in Science*, Springer-Verlag, New York, 1992.
24. Puente, C., J. Romeu, R. Pous, and A. Cardama, "On the behavior of Sierpinski multiband fractal antenna," *IEEE Trans. Antennas Propagat.*, Vol. 46, 517–524, Apr. 1998.
25. Baliarda, C. P., C. B. Borau, M. N. Rodero, and J. Romeu, "An iterative model for fractal antennas: Application to the Sierpinski gasket antenna," *IEEE Trans. Antennas Propagat.*, Vol. 48, 713–719, May 2000.
26. Vinoy, K. J., J. K. Abraham, and V. K. Varadan, "On the relationship between fractal dimension and the performance of multi-resonant dipole antennas using Koch curves," *IEEE Trans. Antennas Propagat.*, Vol. 51, 2296–2303, Sept. 2003.
27. Vinoy, K. J., K. A. Jose, V. K. Varadan, and V. V. Varadan,

"Hilbert curve fractal antenna: A small resonant antenna for VHF/UHF applications," *Microwave and Optical Technology Letters*, Vol. 29, 215–219, 2001.

28. Ataeiseresht, R., C. Ghobadi, and J. Nourinia, "A novel analysis of Minkowski fractal microstrip patch antenna," *Journal of Electromagnetic Waves and Applications*, Vol. 20, No. 8, 1115–1127, 2006.